RSC Advances

PAPER

View Article Online
View Journal | View Issue

Check for updates

Cite this: *RSC Adv.*, 2025, **15**, 39885

Discovery of novel angiotensin-converting enzyme inhibitory peptides by *in silico* and *in vitro* studies

Fenglin Jiao,†[a] Jinlin Yang,†[a] Fangfang Wang,*[a] Shanli Peng*[a] and Bo Zhou[b]

Hypertension represents a crucial risk factor in the development of cardiovascular diseases, including heart failure, stroke, coronary heart disease and myocardial infarction. Currently, synthetic angiotensin-converting enzyme (ACE) inhibitors are an important first-line treatment for hypertension. However, these synthetic ACE inhibitors often produce side effects in clinical application, such as cough, gustatory disturbance and skin rash. Thus, it is urgent to find safe and effective ACE inhibitors for the treatment of hypertension. Therefore, a series of ACE inhibitory peptides were studied using computational approaches. Initially, a reliable 3D-QSAR model was derived based on CoMFA (R_{cv}^2 = 0.660, R_{pred}^2 = 0.6674) and CoMSIA (R_{cv}^2 = 0.646, R_{pred}^2 = 0.6451) methods. Furthermore, molecular docking was also employed to explore the binding mode of the inhibitory peptides at the active site of ACE. At the same time, the ligand-receptor binding characteristics are consistent with the contour map information. Taken together, the derived 3D-QSAR and molecular docking results would offer trustworthy clues for further optimization of this series of ACE inhibitory peptides. Finally, three novel tri-peptides are designed as prospective ACE inhibitors, and the predicted activities by developed 3D-QSAR models, binding affinity by molecular docking, the experimental activity by DOJINDO ACE Kit-WST reagent box all show effective inhibition on ACE.

Received 18th August 2025
Accepted 13th October 2025

DOI: 10.1039/d5ra06104k

rsc.li/rsc-advances

Open Access Article. Published on 21 October 2025. Downloaded on 1/22/2026 4:50:41 AM.
This article is licensed under a Creative Commons Attribution-NonCommercial 3.0 Unported Licence.

1 Introduction

Hypertension is a common cardiovascular disease, which is often associated with functional or organic modifications in the heart, blood vessels, lungs and kidneys. In addition, it is also a significant risk factor for stroke, arteriosclerosis, and coronary heart disease.[1] In the initial stage of hypertension, there are no symptoms until the occurrence of clinical symptoms, such as heart attack, cerebral vascular rupture, and so on, therefore, hypertension is also known as the "silent killer".[2]

Studies have proven that the treatment of hypertension mainly depends on the etiology of the disease, including dietary changes, weight loss, exercise, and drug interventions. It has been demonstrated that drugs are effective in treating hypertension.[3] At present, six main classes of commonly drugs have been employed, including diuretics, β-blockers, calcium antagonists, angiotensin-converting enzyme inhibitor (ACEI), α1-blockers, and angiotensinogen II receptor antagonist (AT1). Nowadays, inhibitors of ACE have been considered as first-line therapy for hypertension.[4]

ACE, a zinc-dependent dipeptidyl carboxylase, plays a regulatory role in the renin-angiotensin system (RAS) and kallikrein-kinin system (KKS). This enzyme can catalyze the conversion of inactive angiotensin I (Ang I, decapeptide) to generate strongly vasoconstrictive angiotensin II (Ang II, octapeptide), and it also can inactivates the vasodilator bradykinin.[5] Therefore, ACE inhibitors serve as the primary and effective medications for treating hypertension and heart failure.[6]

The ACE inhibitor captopril was first discovered in 1981 as a treatment for refractory hypertension.[7] Nowadays, at least 18 ACE inhibitors have been approved for use,[8] including: (1) containing sulfhydryl (–SH) or sulfur (–SR) groups, such as captopril, alacepril; (2) containing carboxyl (–COOH) class, such as enalapril, lisinopril and (3) containing hypophosphonic acid (–POO–) class, such as fosinopril. captopril[9] is the first oral ACE inhibitor to be marketed, which binds to ACE through its unique sulfhydryl group (–SH), the –SH can directly form a strong coordination bond with Zn^{2+} at the active center of ACE. The proline ring binds to the hydrophobic pocket of ACE. Through this dual action, the conversion of Ang I to Ang II is blocked, thereby achieving antihypertensive effect. Lisinopril[10] is one of the few active ACE inhibitors that do not require hepatic metabolism. Its carboxyl group coordinates with Zn^{2+} at the active site of ACE, while the lysine group forms multiple hydrogen bonds with the acidic amino acid residues of ACE. After binding, it continuously blocks the production of Ang II and simultaneously increases bradykinin levels. Fosinopril[11] is

[a]*School of Life Science, Linyi University, Linyi, 276000, China. E-mail: yu100288@163.com*

[b]*State Key Laboratory of Functions and Applications of Medicinal Plants, College of Basic Medical, Guizhou Medical University, Guizhou, 550004, China*

† These authors contributed equally to this work.

© 2025 The Author(s). Published by the Royal Society of Chemistry

Open Access Article. Published on 21 October 2025. Downloaded on 1/22/2026 4:50:41 AM. This article is licensed under a Creative Commons Attribution-NonCommercial 3.0 Unported Licence.

a commonly used clinical drug for the treatment of cardiovascular diseases. As a prodrug, it needs to be hydrolyzed by phosphatase in the liver and intestinal mucosa after oral administration. This hydrolysis converts the dimethyl phosphate group in the molecule into a free phosphate group, generating its active metabolite fosinoprilat. Its core mechanism of action is consistent with that of captopril, by inhibiting the activity of ACE, reducing the production of Ang II, thereby dilating peripheral blood vessels, lowering blood pressure, and improving cardiac load while protecting renal function. The chemical structures of these drugs are shown in Fig. S1. The selectivity of these ACE inhibitors is diverse due to the differences of functional groups. The sulfhydryl and hypophosphonic acid groups have high selectivity to cardiovascular and the carboxyl group is highly selective for kidney.[12]

In the RAS system, ACE inhibitors can block Ang I hydrolysis into Ang II, so that the production of Ang II is reduced, further the blood pressure is lowered. In addition, ACE inhibitors can also reduce vascular dilation by inhibiting the hydrolysis of bradykinin.[13] However, synthetic ACE inhibitors lead to adverse side effects in the form of cough, allergic reactions, taste disturbances, and skin rashes.[14] Researches have indicated that severe cough and loss of taste often occur inexplicably in patients during clinical application. As a result, it is pressing to seek more secure ACE inhibitors.

In recent years, owing to good antihypertensive effect, easy digestibility and high safety, ACE inhibitory peptides have gained extensive attention.[15–17] ACE inhibitory peptides are competitive inhibitors with stronger affinity to the active region of ACE, and are not easily released from the ACE binding region. In 1965, ACE-inhibitory peptides were extracted from snake venom for the first time[18] and these ACE-inhibitory peptides are generally 5–13 amino acids in length, most peptides possess Ala-Pro and Pro-Pro in the C-terminus, and peptide Pyr-Trp-Pro-Arg-Pro-Gln-Ile-Pro-Pro exhibits the best antihypertensive effect for hypertensive animals and has been used *in vitro* to treat human hypertension.[19,20] In 1979, six ACE inhibitory peptides were derived by hydrolyzing gelatin with bacterial collagenase, and this is also the first time that proteases have been used to hydrolyze food proteins *in vitro* to obtain ACE inhibitory peptides.[21] Subsequently, various ACE inhibitory peptides were separated and determined from diverse food proteolytic varieties, such as milk,[22] egg,[23] marine,[24] oat,[25] rapesees,[26] *etc.* The structure–activity relationship of ACE inhibitory peptides shows that the tripeptide at C-terminal strongly affects the binding to ACE, and studies have shown that when amino acids are appropriately extended at the N-terminal of the dipeptide inhibitor, the activity level of the corresponding tripeptide is superior to that of the dipeptide. In addition, ACE has high stereospecificity for the third amino acid at the C-terminus of substrates or inhibitory peptides, which must have an L-configuration, but the stereospecificity for the fourth amino acid is not strict.[27] The activity is also significantly affected by the hydrophobicity of the peptide, studies have proven that high hydrophilicity cannot bring peptide molecules close to the ACE active site, resulting in decreased activity or inactivity. However, the relationship between the structure and activity of these peptides is based on amino acid sequence analysis, and many peptide molecules do not conform to these research results, and the specific structure–activity relationship has not yet been resolved.

Computer-aided drug design is an important tool in modern drug development.[28] With the help of quantitative structure–activity relationships (QSAR),[21,22] it is possible to estimate the activity of new compounds, accelerate the process of development. Therefore, a series of ACE inhibitory peptides were subjected to three dimensional quantitative structure–activity relationship (3D-QSAR) models which were estimated through the application of comparative molecular field analysis (CoMFA) and comparative molecular similarity indices analysis (CoMSIA) approaches. Additionally, molecular docking was also employed to investigate the detailed mode of peptide-ACE interactions. The essential information gathered from the above analyses would be helpful for the design of novel potent ACE inhibitory peptides.

2 Experiments and methods

2.1 Dataset

In order to generate reliable 3D-QSAR models, a collection of ACE inhibitory peptides was retrieved from the literature.[29–32] The inhibitory activities against ACE was expressed as IC_{50}, and IC_{50} (μM) values were firstly converted into the corresponding pIC_{50} ($-\log IC_{50}$) values. These peptides were employed to conduct the 3D-QSAR analysis by dividing the whole dataset into two parts: the training set of 113 peptides was used to develop the model, the test set of 37 compounds was applied to confirm the reliability of the model. The structures and related activities of these peptides were listed in Table 1, * represents the test set compounds.

2.2 Molecular minimization and alignment

Sybyl software was used to conduct the 3D-QSAR models. All peptides were sketched by "biopolymer", and optimized under the Tripos force field,[33] Gasteiger Hückel charges and 0.05 kcal mol^{-1} as a convergence criteria.[34]

For the analysis of CoMFA and CoMSIA, molecular alignment is an essential step.[35,36] In this work, peptide 144 with the highest potency was chosen as a template for molecular alignment. For obtaining trustworthy 3D-QSAR models, two alternative alignment rules, the template ligand-based alignment and the docking-based alignment. For the template ligand-based alignment, the "align database" was employed to align all peptides with the common substructure (denoted in purple), and the resultant alignments of all peptides were illustrated in Fig. 1. Regarding the docking-based alignment, all peptides initially underwent the docking operation and were placed into the binding site of the receptor ACE. Subsequently, the conformations of these docked peptides were utilized for the development of the models. The outcome of the alignment was presented in Fig. S2. However, the findings obtained from the docking structures (R_{pred}^2 ranges from 0.1 to 0.3) were not as good as those from the template ligand-based alignment.

© 2025 The Author(s). Published by the Royal Society of Chemistry

Open Access Article. Published on 21 October 2025. Downloaded on 1/22/2026 4:50:41 AM. This article is licensed under a Creative Commons Attribution-NonCommercial 3.0 Unported Licence.

Table 1 Structure and experimental values of the tripeptide samples

Sequence	Structure	pIC_{50}	Sequence	Structure	pIC_{50}
001	AAP	4.520	076	LGL	4.480
002*	ADA	3.830	077	LIY	6.090
003*	AEL	4.240	078	LKA	5.070
004	AFL	4.200	079	LKP	6.020
005	AGP	3.250	080*	LKY	6.110
006	ALP	3.620	081	LLF	4.100
007*	AQL	4.240	082*	LLL	4.650
008	AVP	3.470	083	LLP	4.800
009*	DLP	5.320	084	LPF	4.400
010	FAL	4.580	085	LPP	5.020
011*	FCF	4.960	086	LRP	6.210
012	FDK	3.410	087	LQP	5.830
013	FEP	4.920	088*	LQW	5.420
014	FFF	4.800	089	LSA	5.110
015*	FFG	3.290	090	LSP	5.770
016	FFL	4.430	091	LTF	5.560
017*	FFP	4.920	092	LVL	5.190
018	FGF	4.710	093	LVQ	4.850
019	FGG	3.210	094*	LVR	4.850
020*	FGK	3.800	095	LVY	5.740
021	FIV	3.960	096	LWA	4.900
022*	FNF	5.160	097	LWY	5.300
023*	FPF	4.680	098*	LYP	5.180
024	FPK	3.550	099	MNP	4.180
025	FPP	4.500	100*	PFP	4.260
026	FQP	4.920	101*	PGI	3.770
027*	FWN	4.740	102	PGG	2.860
028	FYN	4.740	103	PGL	4.860
029*	GEG	3.720	104*	PGP	4.180
030	GFF	4.980	105	PGR	3.330
031	GFG	3.470	106	PIP	4.310
032	GGF	4.890	107	PLW	4.440
033	GGG	3.390	108	PPG	2.820
034	GGP	4.720	109	PPP	4.140
035	GKV	5.410	110*	PSY	4.800
036*	GLG	3.550	111*	PWP	3.660
037	GLY	5.050	112	PYP	3.660
038*	GPL	5.590	113	PFH	3.480
039	GPM	4.770	114*	RGP	4.270
040*	GPP	4.920	115*	RPG	2.910
041*	GQP	5.490	116	RPP	4.220
042	GRP	4.700	117	RRR	4.230
043*	GSH	4.490	118*	SVY	5.090
044	GVV	4.180	119	TNP	3.680
045	GYG	3.670	120	VAA	4.890
046	GYY	4.930	121	VAF	4.450
047	HIR	3.020	122	VGP	4.580
048	HLL	4.240	123	VIY	5.120
049	HQG	3.130	124	VLP	4.090
050	IAE	4.460	125*	VLY	4.510
051	IAP	5.570	126	VPP	5.050
052	IAQ	4.460	127*	VQV	5.060
053	IFL	4.350	128	VRP	5.660
054	IKP	5.680	129	VSP	5.000
055	IKY	6.680	130	VSW	4.630
056	ILP	4.490	131	VTR	3.870
057	IMY	5.740	132	VVF	4.450
058	IPA	3.850	133*	VVV	4.370
059	IPP	5.300	134*	VWY	5.030
060	IRA	5.010	135	VYP	3.830
061	IRP	5.740	136	YPF	4.400
062	ITF	4.310	137	YPR	4.780
063	IVQ	4.020	138*	YYY	4.460

Table 1 (*Contd.*)

Sequence	Structure	pIC_{50}	Sequence	Structure	pIC_{50}
064	IVY	5.840	139	AMY	5.260
065	IWH	5.460	140	FAP	5.420
066	IYP	4.210	141	GGY	5.890
067	KPF	4.490	142	HHL	5.270
068	LAA	4.890	143*	IKW	6.680
069	LAP	5.730	144	LRY	6.820
070*	LAY	5.410	145	MKY	5.140
071	LDP	4.370	146	PRY	5.600
072	LEE	4.000	147	RIY	4.550
073	LEL	4.810	148	TVY	4.820
074	LEP	5.240	149	VAP	5.700
075	LGI	4.540	150	YEY	5.400

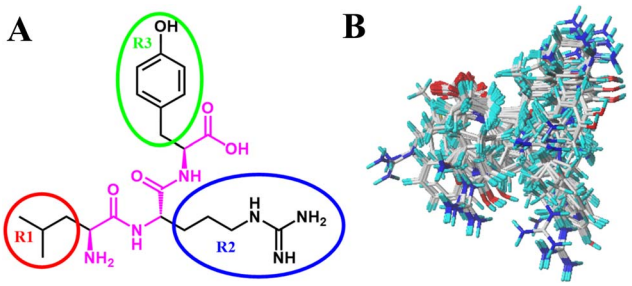

Fig. 1 (A) Structure of peptide 144, the common substructure is shown in purple. (B) Aligned dataset of the whole peptides by choosing peptide 144 as the template.

Consequently, only the models that originated from the template ligand-based alignment were subjected to analysis.

2.3 3D-QSAR analysis

CoMFA and CoMSIA methods were all built on the concept of different fields surrounding the aligned peptides.[37] The calculation of the CoMFA model involved the use of steric (Lennard–Jones potentials) and electrostatic (Coulomb potentials) fields. A sp^3 hybridized carbon atom with a Van Der Waals radius of 1.52 Å and a charge of +1 was used as part of this calculation. Also, the energy cutoff was fixed as the standard value of 30 kcal mol^{-1}.[35]

For the CoMSIA method,[36] the calculation of the steric, electrostatic, hydrophobic, hydrogen bond donor, and hydrogen bond acceptor fields is carried out with the same parameters as those in the CoMFA analysis. Also, the value for column filtering was established at 2.0 kcal mol^{-1}, while the energy cutoff values value was set at 30 kcal mol^{-1}.

Partial least squares (PLS) was conducted to investigate the relationship between CoMFA and CoMSIA descriptors and inhibitory activities.[38] Employing the leave-one-out (LOO) cross-validation method, the cross-validated correlation coefficient (R_{cv}^2) and the optimal number of components (Nc) were identified. After that, non-cross validation, with the use of the obtained Nc, was applied to calculate the non-cross-validated

Open Access Article. Published on 21 October 2025. Downloaded on 1/22/2026 4:50:41 AM. This article is licensed under a Creative Commons Attribution-NonCommercial 3.0 Unported Licence.

correlation coefficient (R_{ncv}^2), F value, standard error of estimation (SEE), and the contribution value of each field. The R_{cv}^2 and R_{ncv}^2 values define the internal uniformity of the model and the internal predictive aptitude of the model, respectively. The models with high values of R_{cv}^2 ($R_{cv}^2 > 0.5$) as well as the R_{ncv}^2 ($R_{ncv}^2 > 0.5$) and low values of SEE are regarded as predictive models.

For the purpose of appraising the predictive potential of the 3D-QSAR models constructed from the training set, the inhibitory activities of the peptides within the test set were predicted. Afterward, the predicted correlation coefficient (R_{pred}^2) based on Golbraikh and Tropsha validation was examined, and the definition is presented as follows:

$$R_{pred}^2 = \frac{(SD - PRESS)}{SD} \quad (1)$$

where PRESS is the quadratic difference between the experimental and predicted activities of the peptides in the test set, and the SD is the total of the squared deviation between the activities in the test set and the mean activity of the training set.

2.4 Applicability domain (AD)

Applicability domain is defined as the similarity of the predicted compounds to those in the training set.[39,40] When all compounds situated within the applicability domain, the developed models are regarded as reliable. In this study, we chose a reliable method to calculate the AD, which was achieved through the following link: **http://dtclab.webs.com/softwaretools** or **http://teqip.jdvu.ac.in/QSAR_Tools/**.

2.5 Molecular docking

Molecular docking is a widely used approach that can help us understand the binding mode of a ligand to a protein.[41,42] In this study, the AutoDock software was conducted for molecular docking. The receptor ACE was obtained from the RCSB PDB (**https://www.rcsb.org/**) with PDB ID 3BKK, which was determined by X-ray diffraction at a resolution of 2.17 Å. Prior to molecular docking, the ions and water molecules in the crystal structure 3BKK were deleted, and the Kollman charges and polar hydrogen were assigned to the protein.[43] The AutoGrid algorithm[43] was employed to generate a 3D grid, which was utilized to assess the interaction energy between the ligand and the protein ACE. For the molecular docking process, we defined the docking site using a grid box with dimensions of 60 × 60 × 60 Å, a grid spacing of 1 Å, and Cartesian [x, y, z] coordinates of [46.129, 44.457, 45.34]. We carried out 100 runs based on the genetic algorithm to select an appropriate conformation. The derived conformations were also used in constructing the docking-based 3D-QSAR models. Furthermore, to validate the reliability of molecular docking, we performed a re-docking procedure, the root mean square deviation (RMSD) between the original and re-docked conformations should be lower than 2.0 Å.[44,45]

2.6 Synthesize the designed peptides

The peptides were synthesized *via* the Fmoc solid-phase synthesis method. The synthesis process is composed of the following several cycles:

(1) Deprotection: to eliminate the protecting group of the amino group, both the Fmoc-protected column and monomers need to be treated with an alkaline solvent namely piperidine.

(2) Activation and cross-linking: the carboxyl group of the next amino acid is activated by an activator. The activated monomer reacts and cross-links with the free amino group to form a peptide bond. In this step, a large amount of super-concentrated reagent is used to drive the reaction to completion. Cycle: these two reactions are repeated in cycles until the synthesis is completed.

(3) Elution and deprotection: the peptides are removed from the column through elution. Subsequently, the protecting groups are removed by subjecting them to a deprotecting agent (TFA), which both elutes and deprotects the peptides.

2.7 *In vitro* ACE inhibitory activity analysis of the designed peptides

The ACE inhibitory activity of the designed peptides was determined using the DOJINDO ACE Kit-WST reagent box, and the analysis method was same as that of the reagent box method. An ACE inhibitory activity curve was made based on the sample concentration and inhibition rate, and the sample concentration (IC_{50}) at an inhibition rate of 50% was calculated.

3 Results and discussion

3.1 3D-QSAR models

The CoMFA and CoMSIA approaches were used to establish the relationship between the three dimensional structure and inhibitory activities of the peptides. The statistical parameters for derived 3D-QSAR models are presented in Table 2.

The results indicate that CoMFA model exhibits a relatively high cross-validated correlation coefficient ($R_{cv}^2 = 0.660$), a non-cross-validated correlation coefficient ($R_{ncv}^2 = 0.828$), a standard error of estimation (SEE = 0.251) with an optimal

Table 2 Statistical Data of Optimal QSAR Models

								Fields contribution				
Model	R_{cv}^2	R_{ncv}^2	SEE	F	R_{pred}^2	SEP	Nc	S	E	H	D	A
CoMFA	0.660	0.828	0.251	102.984	0.6674	0.361	5	0.713	0.287	—	—	—
CoMSIA	0.646	0.875	0.304	90.586	0.6451	0.378	8	0.299	—	0.452		0.249

© 2025 The Author(s). Published by the Royal Society of Chemistry

Open Access Article. Published on 21 October 2025. Downloaded on 1/22/2026 4:50:41 AM.
This article is licensed under a Creative Commons Attribution-NonCommercial 3.0 Unported Licence.

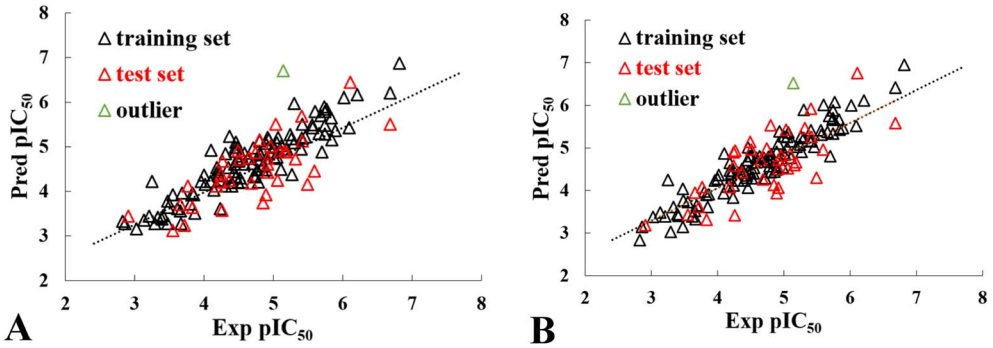

Fig. 2 Linear regression between the experimental and predicted activities for the training and test set of the peptides by (A) CoMFA model. (B) CoMSIA model.

number of principal components (Nc = 5). The value of R_{cv}^2 and R_{ncv}^2, along with the low SEE value, demonstrate that the constructed CoMFA model is reliable and has good internal predictive ability. Regarding the percentage contribution of CoMFA descriptors, the steric contributes 71.3% and the electrostatic contributes 28.7%. This clearly indicates that the steric contribution is more substantial than the electrostatic one. Additionally, the high predicted correlation coefficient (R_{pred}^2 =0.6674) implies that the model can effectively predict the properties of external test set compounds. As depicted in Fig. 2A, there exists a statistical relationship between the experimental pIC_{50} values and the values predicted by the CoMFA model. The figure visually demonstrates the degree of alignment between the predicted and actual data.

To study the impact of each CoMSIA field on prediction ability, a comprehensive analysis of all combinations of CoMSIA descriptors is conducted (Table S1). The results are validated by R_{cv}^2 and R_{pred}^2 values, as depicted in Fig. 3. This process has identified that that most influential CoMSIA model is based on the combination of steric, hydrophobic, and hydrogen bond acceptor descriptors. The outcomes of Table 2 also point out that CoMSIA-SHA model has high R_{cv}^2 of 0.646, R_{ncv}^2 of 0.875, 0.304 as standard error of estimation (SEE), F value of 90.586, and Nc of 8, implying that the prediction accuracy of the CoMSIA model is within an acceptable range. The proportions of steric, hydrophobic, and hydrogen bond acceptor contributions account for 29.9%, 45.2%, and 24.9%, respectively, showing that the hydrophobic field creates the higher contribution to the inhibitory activity. The CoMSIA model also has been validated by the reserved test set, and the R_{pred}^2 is calculated to be 0.6451. The linear fit plot in Fig. 2B shows the linear relationship between the experimental and predicted values in the data set of the CoMSIA model. The predicted activities are in high accordance with the experimental data, indicating that the CoMSIA model has a desirable potential and can be employed for the design of novel molecules.

In addition, the applicability domain (AD) was also computed, and the results show that no outliers among the training set and test set peptides for CoMFA and CoMSIA-SHA models. This suggests the dependability of the developed 3D-QSAR models.

3.2 Contour map analysis

Contour map analysis is carried out for the most active peptide 144 at specific spatial areas to understand the essential molecular criteria. The contour maps can be employed to visualize the favorable and unfavorable areas in which the structural modifications of the molecule cause an increase or decrease in inhibitory activity.

3.2.1 CoMFA contour map. The contour maps around peptide 144 for steric field based on CoMFA model can be seen in Fig. 4A. The green regions signify the significance of bulky groups in promoting the inhibitory activities, and the yellow contours indicate regions where bulky substituents are unfavorable for the activity. Several yellow contours are found around the first amino acid (N-terminal position), suggesting

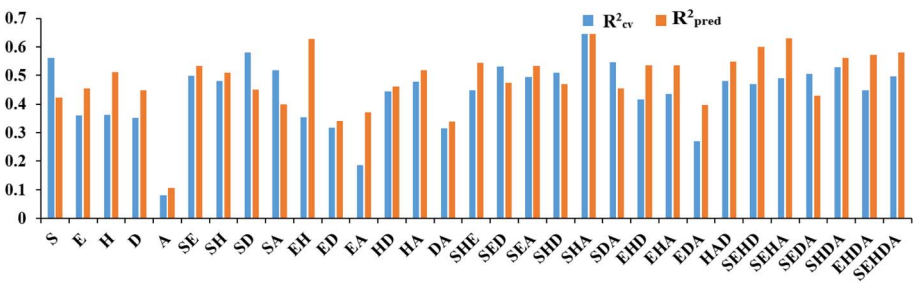

Fig. 3 Diagram of different combination of CoMSIA descriptors with the corresponding R_{cv}^2 and R_{pred}^2 values.

Open Access Article. Published on 21 October 2025. Downloaded on 1/22/2026 4:50:41 AM.
This article is licensed under a Creative Commons Attribution-NonCommercial 3.0 Unported Licence.

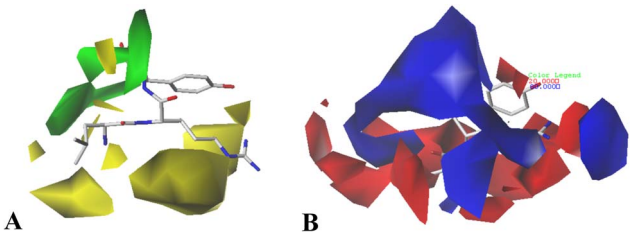

Fig. 4 CoMFA contour maps in combination with peptide 144. (A) Steric field, where the green and yellow contours represent 80% and 20% level contributions, respectively. (B) Electrostatic field, where the blue and red contours represent 80% and 20% level contributions, respectively.

the small groups are favored in this region. The activity increases as the molecule become smaller in this region, for example, the activity of peptide 138 (Tyr) is lower than peptide 46 (Gly), and a similar trend is observed for peptides 40 (Gly) and 116 (Arg), 40 ($pIC_{50} = 4.920$) > 116 ($pIC_{50} = 4.220$). Several yellow contours close to the second amino acid (N-terminal) recommend that small size group at this position has a beneficial effect on inhibition. For instance, comparing peptides 69 and 71, the inhibitory activity of peptide 69 (Ala) is higher than that of peptide 71 (Asp). Moreover, the third amino acid Tyr is adjacent to yellow contour maps, which indicate that adding bulkier substituents there would reduce the inhibitory activity. This agrees with the smaller value of peptide 121 (Phe) compared with peptide 120 (Ala).

Fig. 4B displays the electrostatic contour maps, where the blue and red contours correspond to the electropositive and electronegative charges favored region, respectively. The first amino acid at the N-terminal is surrounded by red contours, implying that the inhibitory activity would be enhanced when the electronegative groups introduced. This could explain why the activity of peptide 009 (Asp) is higher than that of peptide 006 (Ala). A large blue area is found near the second amino acid, indicating that electropositive groups at this position would increase the activity, this situation could be explained by the fact that the pIC_{50} value of peptide 86 (Arg) is greater than that of peptide 85 (Pro). Furthermore, some red contours around the third amino acid illustrate that electronegative substituents are required at this area. This is in line of the higher activity of peptide 95 with Tyr than that of peptide 94 with Arg.

3.2.2 CoMSIA contour map. As can be seen in Fig. 5A, the CoMSIA steric contour maps are similar to the CoMFA ones (Fig. 4A), for example, the first amino acid and the third amino acid (N-terminal) are covered by yellow contours. In contrast, a green contour map is located near the third amino acid, illustrating that the volume of substituent at this position should be considered carefully.

In the CoMSIA hydrophobic contour map (Fig. 5B), the yellow contour map represents the hydrophobic groups are favorable for the activity, on the other hand, the grey contour map represents hydrophilic groups favored region. There are yellow contour maps at the first amino acid (N-terminal), so introducing a hydrophobic group here will enhance the activity, peptides 40, 126, and 59 with hydrophobic residues Gly, Val, and Ile at this location reveal higher activities than peptide 116 with Arg. A grey contour near the second amino acid hints that incorporating of hydrophilic group at this position could be advantageous for enhancing the inhibitory activity. This accounts for why peptide 86, which contains the hydrophilic amino acid Arg, is more active than peptide 85, which has the hydrophobic residue Pro. Furthermore, we noticed a grey contour encompassing the third amino acid Tyr. This implies that hydrophilic substituents are necessary in this region. This is demonstrated by the fact that peptide 20, with Lys at this position, shows higher activity than peptide 19, which has Gly. Additionally, this aligns with the inhibitory activity trend: peptide 137 (Arg) > peptide 136 (Phe).

In the CoMSIA model, Fig. 5C presents the hydrogen bond acceptor contour maps. These maps display regions in magenta (hydrogen bond acceptors favorable) and red (hydrogen bond acceptor unfavorable). A magenta map is found around the first amino acid Leu, suggesting that hydrogen bond acceptor groups are more suitable in this location. This finding helps to explain why the pIC_{50} of peptide 9 with Asp is higher than pIC_{50} of peptide 6 (Ala). The maps also reveal a red contour at the second amino acid Arg, indicating that the presence of hydrogen bond donor groups in this area would enhance the ACE inhibitory activity. This is corroborated by the fact that peptide 60, with residue Arg, has higher activity than peptide 58 with Pro. Furthermore, a magenta contour map is located near the third amino acid Tyr, indicates that the use of hydrogen bond acceptor groups in this vicinity can boost the activity. As a result, peptide 90, with Pro, exhibits higher activity then peptide 89, with Ala.

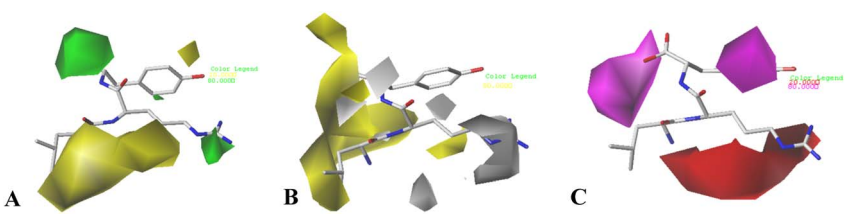

Fig. 5 CoMSIA contour maps in combination of peptide 144. (A) Steric field, where the green and yellow contours represent 80% and 20% level contributions, respectively. (B) Hydrophobic field, where the yellow and grey contours represent 80% and 20% level contributions, respectively. (C) Hydrogen bond acceptor field, where the magenta and red contours represent 80% and 20% level contributions, respectively.

© 2025 The Author(s). Published by the Royal Society of Chemistry

Open Access Article. Published on 21 October 2025. Downloaded on 1/22/2026 4:50:41 AM.
This article is licensed under a Creative Commons Attribution-NonCommercial 3.0 Unported Licence.

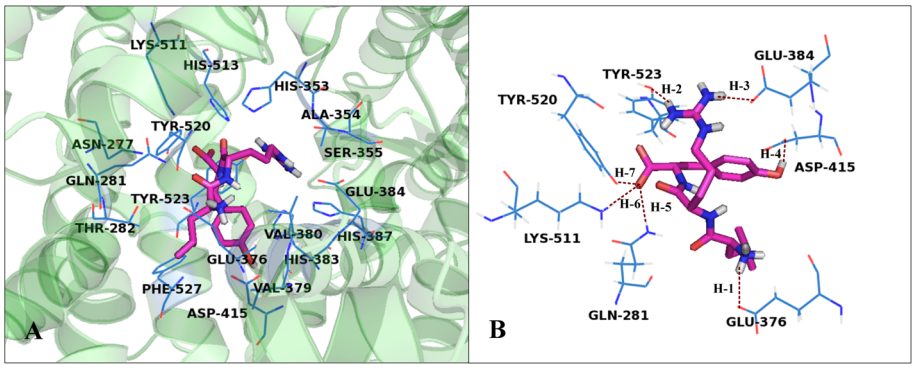

Fig. 6 (A) Position of the best conformation of the peptide 144 in the binding pocket of ACE receptor (the amino acid residues within 4.5 Å are displayed). (B) The hydrogen bond interactions of peptide 144 with receptor ACE, hydrogen bond is shown in black dotted line.

3.3 Molecular docking

Initially, the reliability and effectiveness of the molecular docking protocol have been validated *via* the re-docking procedure. As illustrated in Fig. S3, the re-docked conformation (displayed in magenta) exhibits a high degree of overlap with the native ligand (shown in red), yielding a root mean square deviation (RMSD) of 0.26 Å. This value falls well within the acceptable threshold of 2 Å, as established in previous literature,[46] further validating the reliability of the parameters employed in the molecular docking process.

After the validation of molecular docking and the conformation of the active site, the most active peptide 144 is chosen to visualize the interactions between the receptor ACE and the ligand. Fig. 6A displays that peptide 144 is surrounded by essential amino acid residues Asn277, Gln281, Thr282, His353, Ala354, Ser355, Glu376, Val379, Val380, His383, Glu384, His387, Asp415, Lys511, His513, Tyr520, Tyr523, and Phe527. The powerful biding of the peptide to the binding site of ACE is further aided by hydrogen bond interactions (Fig. 6B): (1) the –NH_2 of the first amino acid Leu forms hydrogen bond with Glu376 (–O···HN, 2.14 Å, 99.0°) (H-1); (2) the second amino acid Arg serving as hydrogen bond donor creates two hydrogen bonds with Tyr523 (–O···HN, 2.23 Å, 156.9°) (H-2) and Glu384 (–O···HN, 2.05 Å, 152.6°) (H-3), this is consistent with the red contour map illustrated in Fig. 5C; (3) the third amino acid residue Tyr shows four conventional hydrogen bonds with Asp415 (–O···HO, 1.85 Å, 167.9°) (H-4), Gln281 (–O···HN, 2.06 Å, 153.5°) (H-5), Lys511 (–O···HN, 1.89 Å, 165.3°) (H-6), and Tyr520 (–O···HO, 1.89 Å, 148.2°) (H-3). Additionally, arene–arene interactions are formed by the benzene ring of the third amino acid Tyr, thereby enhancing the binding activity. In addition, the second amino acid residue Arg is located in a small binding site and is adjacent to hydrophilic amino acids His353, Ser355, His383, Glu384, His387, His513, and Tyr523, indicating that minor and hydrophilic substituents at this position are desired, this is in accord with the yellow and grey contour maps as shown in Fig. 4A and 5B. Furthermore, the side chain –OH of the third amino acid Tyr forms hydrogen bond with Asp415, hinting that the group in this region should be minor, otherwise, it will conflict with the surrounding amino acids, which is corroborated by the yellow contour (Fig. 4A). On the contrary, the benzene ring of the third amino acid lies in a large binding pocket, suggesting that bulky groups are required, which is coincident with the green contour map presented in Fig. 5A. For specific details, the third amino acid Tyr is placed into a binding pocket with hydrophilic residues His383, Asp415, and Tyr523, supporting the CoMSIA hydrophobic grey contour map (Fig. 5B). Comparing the docking results and the CoMFA/CoMSIA contour maps further validates the success of the docking process and the reliability of the 3D-QSAR models.

Additionally, several more potent and lower ACE inhibitory peptides were chosen to analyze the structure–activity relationship, the results are shown in Table S3. Peptides with higher activities (144, 143, 055, 086, 080, 077, 079) generally form multiple hydrogen bonds with amino acids in ACE proteins. For instance, most of them form hydrogen bonds with amino acids such as Gln281, Glu384, Asp415, and Tyr520. These amino acids may play important roles in the active site of ACE or in key regions involved in substrate binding. Gln281 has a polar side chain and can form hydrogen bonds, helping stabilize the binding of peptide molecules to ACE. Glu384 and Asp415 possess negative charges and can form strong hydrogen bonds with positively charged groups in peptide molecules or hydrogen atoms with appropriate orientations, thereby enhancing the binding force. The phenolic hydroxyl group of Tyr520 can participate in the formation of hydrogen bonds, contributing to the binding specificity and stability. However, peptides with lower activities (108, 102, 115, 047, 049, 019, 005) form relatively fewer hydrogen bonds, or interact with fewer types of amino acids *via* hydrogen bonding. For example, molecule 108 forms hydrogen bonds only with Gln281. This indicates that insufficient hydrogen bond interactions may fail to provide strong enough binding force, resulting in unstable binding between peptide molecules and ACE, which in turn leads to lower activity.

Secondly, the peptides with higher activity (144, 143, 055) all exhibit π–π interactions with His383. These interactions increase the binding energy between the peptides and ACE, thereby contributing to the enhancement of the activity. In contrast, molecules with lower activity do not show π–π interactions, which in turn lead to a decreased activity.

Open Access Article. Published on 21 October 2025. Downloaded on 1/22/2026 4:50:41 AM.
This article is licensed under a Creative Commons Attribution-NonCommercial 3.0 Unported Licence.

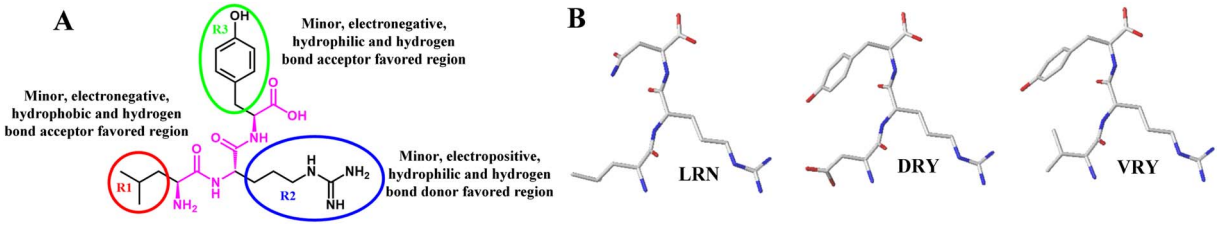

Fig. 7 (A) Structure–activity relationship obtained from 3D-QSAR studies; (B) structures of newly designed peptides.

Table 3 Structures and activities of newly designed peptides

Number	Amino acid sequence	CoMFA	CoMSIA
D1	LRN	6.828	6.851
D2	DRY	7.027	6.856
D3	VRY	6.930	6.897

3.4 Design of novel peptides

The principal aim of the present work is the design of novel peptides, through the recommendations extracted from 3D-QSAR and molecular docking on the structural characteristics of the potent peptide 144 (Fig. 7). In this work, several tri-peptides are designed to find novel ACE inhibitors, and the newly designed peptides are aligned to the original database, and we use the optimum CoMFA and CoMSIA models to predict the activities of the newly designed peptides (Fig. 7). The new peptides with inhibitory activities are shown in Table 3.

3.5 Synthesize the designed peptides

The peptides synthesized by the Fmoc solid-phase synthesis method have relatively high yield and the products have relatively high purity. The synthesized peptides were separated by semi-preparative high-performance liquid chromatography, and verified by mass spectrometry (MS) and high performance liquid chromatography (HPLC), as shown in Fig. 8, 9 and Tables S4–S6. In addition, the synthetic steps and conditions for D1, D2 and D3 are listed in Fig. S4–S6. The purity of the peptide D1, D2 and D3 is 98.14%, 99.68%, and 99.94%, respectivley. Furthermore, the yeild of the designed peptdes is approximately 1.2%. In addition, to validate the behavior of the designed peptides to be good ACE candidates, a study of the pharmacokinetic properties of the newly developed peptides was carried out by online tool admetSAR (**http://lmmd.ecust.edu.cn/admetsar1/**). The results of the properties are shown in Table S7, indicating that the designed peptides have potential as ACE inhibitors.

3.6 Molecular docking of the designed peptides

Using the same docking protocol, all the designed peptides were docked into the active site of the target receptor ACE. As listed in Table 4, the docking results indicate that all the three designed peptides exhibit higher binding affinity than the most potent peptide 144.

The modes of the interaction obtained for D1, D2, and D3 are shown in Fig. 10–12. As shown in Fig. 10A, the peptide D1 is surrounded by amino acid residues Asn66, Asn70, His353, Ala354, Ser355, Ala356, Trp357, Lys368, His383, Glu384, His387, Phe391, His410, Glu411, Phe512, His513, Arg522, and Tyr523. In addition, the peptide D2 mainly interacts with amino acids Glu162, Gln281, His353, Ala354, Ser355, Glu376, Asp377, Val379, Val380, His383, Glu384, His387, Glu411, Asp415, Lys454, Phe457, Lys511, His513, Tyr520, Tyr523, and Phe527 (Fig. 11A). Furthermore, the peptide D3 forms interactions with Gln281, Thr282, His353, Ala354, Ser355, Ala356, Glu376, Val379, Val380, His383, Glu384, His387, Glu411, Asp415, Lys454, Phe457, Lys511, His513, Tyr520, Tyr523, and Glun530 (Fig. 12A). The binding situation illustrates that all the designed peptides are fell in the same active pocket of the receptor, there are only differences in the binding orientations.

The interaction results of D1 and ACE (Fig. 10B) provides hydrogen bond interactions with Ala356 (–O···HN, 1.90 Å, 153.7°) (–O···HN, 2.17 Å, 142.9°), His387 (–N···HN, 2.03 Å, 149.6°), His383 (–N···HN, 2.32 Å, 105.9°) (–N···HN, 2.69 Å, 105.3°), Glu384 (–O···HN, 1.97 Å, 143.7°), Glu411 (–N···HN, 2.04 Å, 142.2°), Tyr523 (–O···HN, 1.85 Å, 171.6°), Asn66 (–O···HN, 2.02 Å, 169.4°), Ser355 (–O···HO, 1.90 Å, 152.9°). It can be seen that three are seven hydrogen bonds between D2 and ACE (Fig. 11B): Asp377 (–O···HN, 2.03 Å, 156.9°), Glu384 (–O···HN, 1.98 Å, 162.8°), His387 (–O···HN, 2.10 Å, 159.1°) (–N···HN, 2.33 Å, 147.4°), Glu411 (–O···HN, 2.22 Å, 109.1°), Tyr523 (–O···HN, 1.95 Å, 153.0°) (–O···HN, 2.12 Å, 149.8°). Additionally, arene–arene interaction is also established between His383 and the benzene ring of Tyr. It is also reported that hydrogen bonds are also formed between D3 and Glu384 (–O···HN, 1.73 Å, 162.8°) (–O···HN, 2.17 Å, 172.3°), Tyr523 (–O···HN, 2.06 Å, 146.5°), Lys511 (–O···HN, 1.71 Å, 140.9°), Tyr520 (–O···HO, 1.76 Å, 171.6°), Asp415 (–O···HO, 2.03 Å, 172.6°) (Fig. 12B). From the molecular docking analysis, it is appeared clearly that the designed peptides showed important binding modes to the ACE receptor, and hydrogen bond interactions provide positive impact on the inhibitory potency. In addition, it also confirms the effectiveness of the constructed 3D-QSAR models.

3.7 The results of *in vitro* ACE inhibitory activity analysis of the designed peptides

In the ACE inhibition assay, the positive control captopril exhibits a concentration-dependent inhibitory effect on ACE,

© 2025 The Author(s). Published by the Royal Society of Chemistry

Open Access Article. Published on 21 October 2025. Downloaded on 1/22/2026 4:50:41 AM.
This article is licensed under a Creative Commons Attribution-NonCommercial 3.0 Unported Licence.

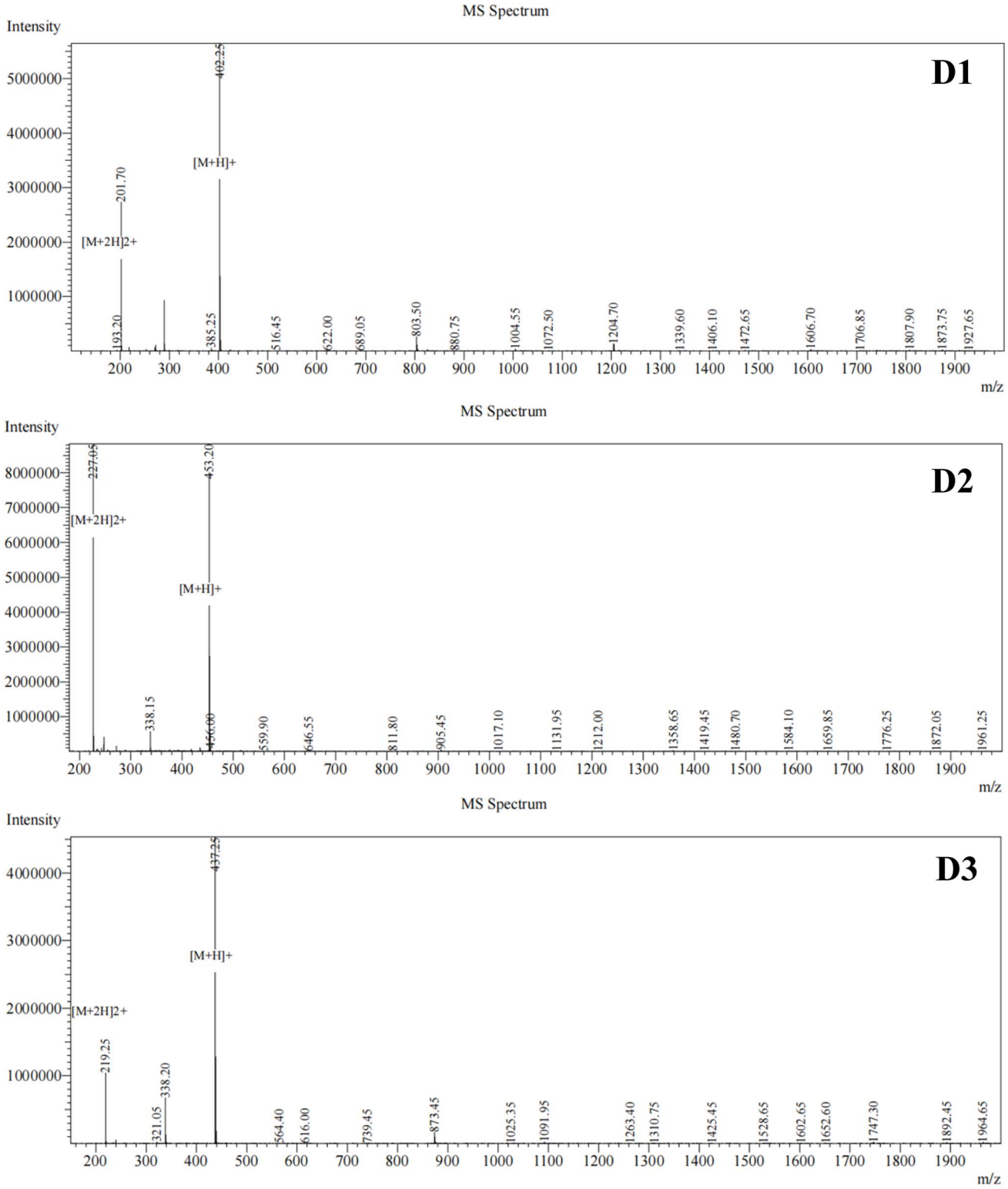

Fig. 8 The mass spectrometry for the designed peptides.

a calculated IC_{50} of 0.032 ± 0.002 μmol (mean ± SD, $n = 3$), with a 28% relative deviation from the literature-reported 0.025 μmol.[47] This discrepancy falls within the acceptable 20–30% biological variability range for ACE inhibitor IC_{50} assays, thus confirming the reliability of the experiment. The inhibitory effects of designed peptides and captopril on ACE

Open Access Article. Published on 21 October 2025. Downloaded on 1/22/2026 4:50:41 AM. This article is licensed under a Creative Commons Attribution-NonCommercial 3.0 Unported Licence.

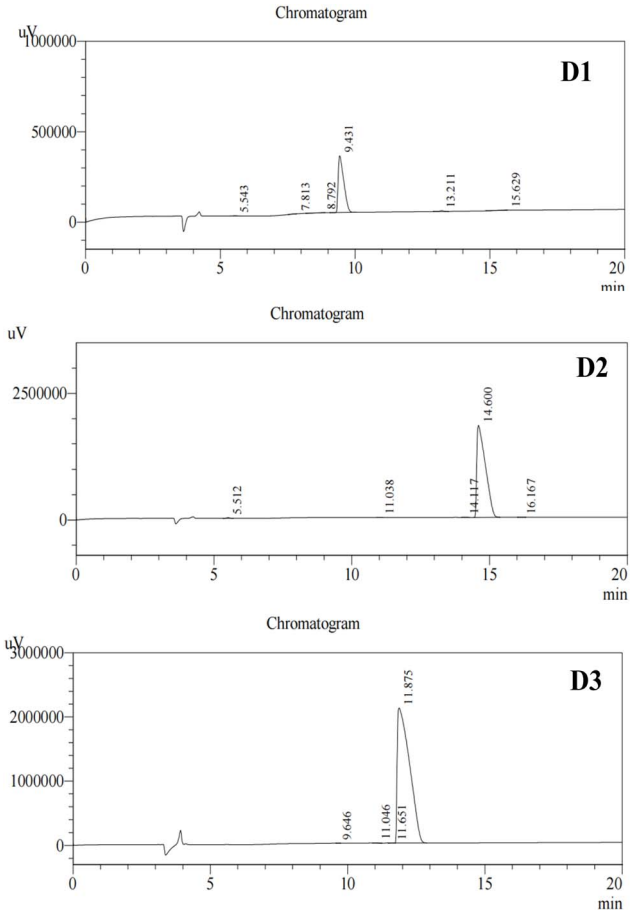

Fig. 9 The high performance liquid chromatography for the designed peptides.

Table 4 The docking results of the designed peptides and the template peptide

Number	Affinity (kcal mol^{-1})
Peptide 144	−9.8
D1	−10.3
D2	−11.4
D3	−12.7

activity are shown in Fig. 13, Table S8 and S9. As shown in Fig. 13, D1, D2, D3 and captopril all exert a noticeable inhibitory effect on ACE activity, and the inhibition rates increases progressively with the rise in mass concentration, indicating a clear concentration-dependence pattern. Within the tested concentration range, D3 exhibits the most potent ACE-inhibitory activity, with an IC_{50} value of (0.078 ± 0.004) μmol, which is significantly superior to those of the other two peptides D1 and D2 ($P < 0.05$). D1 and D2 show weaker ACE-inhibitory activities, with IC_{50} values of (0.129 ± 0.006) μmol and (0.112 ± 0.006) μmol, respectively; nevertheless, their potencies are still higher than that of compound 144, the most active compound reported in this work.

Under identical assay conditions, captopril is approximately 2.4 times more potent than peptide D3 (VRY). The higher activity of captopril stems from the thiol (–SH) group, which forms a strong coordinate bond with the Zn^{2+} ion in the ACE active site, as well as the specific binding of its proline ring to the hydrophobic pocket of ACE. Being devoid of a thiol, D3 mainly relies on non-covalent interactions: the guanidinium of the Arg residue establishes electrostatic interactions with acidic residues (*e.g.*, Glu376, Asp415, Glu384) in the ACE active pocket, while the phenolic hydroxyl of Tyr forms a hydrogen bond to Asp415. Collectively, these forces are slightly weaker than the thiol-Zn^{2+} coordination, resulting in a slightly higher IC_{50} value than that of captopril. Furthermore, captopril is a small molecule containing a rigid proline ring, which can be accurately embedded into the hydrophobic cavity of ACE with high spatial matching. In contrast, peptide D3 as a linear tripeptide, possesses intrinsic flexibility that may populate conformations less compatible with the pocket, further reducing binding efficiency. Nevertheless, with an IC_{50} < 0.1 μmol, D3 still qualifies as a "potent ACE inhibitor". This potency is attributed to the cooperative engagement of Arg (guanidino group), Tyr (phenolic hydroxyl group) and Val (hydrophobic group) in ACE recognition. In summary, although the activity of peptide D3 is slightly less active than captopril, its low toxicity, high biocompatibility, small molecular weight and good absorbability offer a new direction for the development of "safe ACE inhibitors" and make up for the slight gap in activity values.

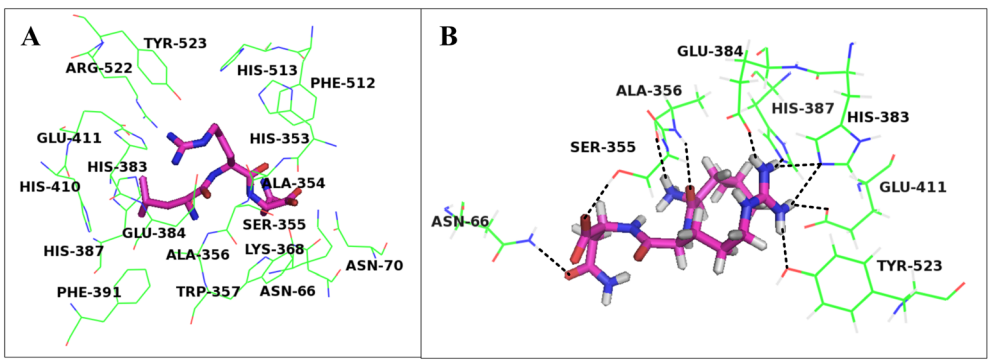

Fig. 10 (A) Position of the best conformation of D1 in the binding pocket of ACE receptor (the amino acid residues within 4.5 Å are displayed). (B) The hydrogen bond interactions of D1 with receptor ACE, hydrogen bond is shown in black dotted line.

© 2025 The Author(s). Published by the Royal Society of Chemistry

Open Access Article. Published on 21 October 2025. Downloaded on 1/22/2026 4:50:41 AM.
This article is licensed under a Creative Commons Attribution-NonCommercial 3.0 Unported Licence.

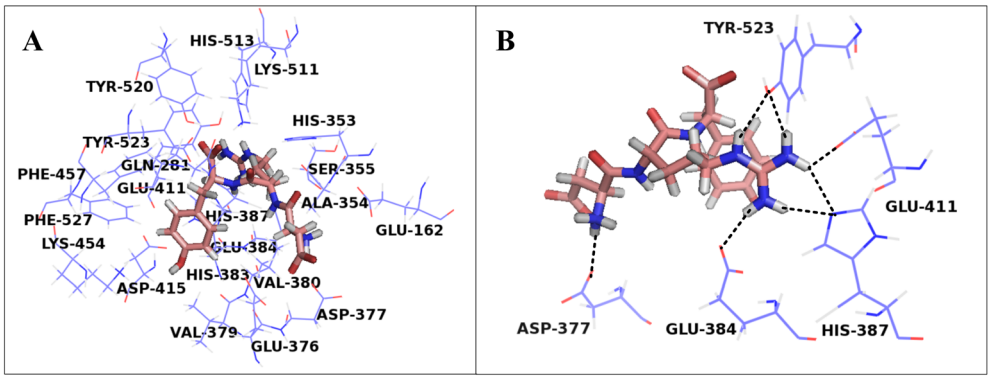

Fig. 11 (A) Position of the best conformation of D2 in the binding pocket of ACE receptor (the amino acid residues within 4.5 Å are displayed). (B) The hydrogen bond interactions of D2 with receptor ACE, hydrogen bond is shown in black dotted line.

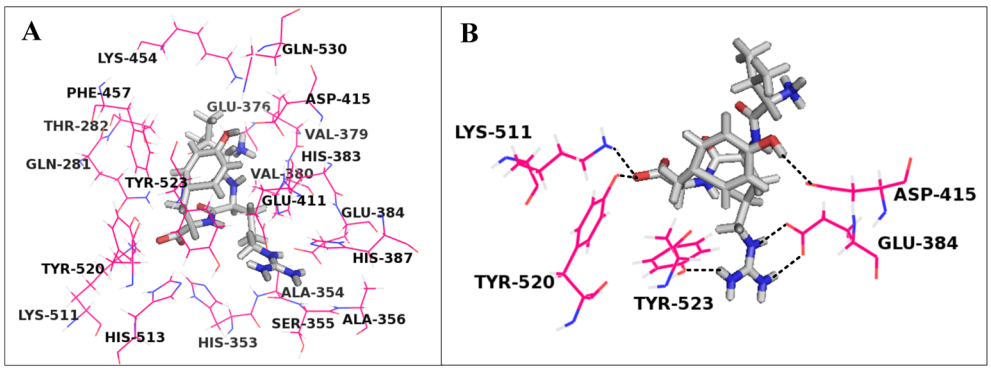

Fig. 12 (A) Position of the best conformation of D3 in the binding pocket of ACE receptor (the amino acid residues within 4.5 Å are displayed). (B) The hydrogen bond interactions of D3 with receptor ACE, hydrogen bond is shown in black dotted line.

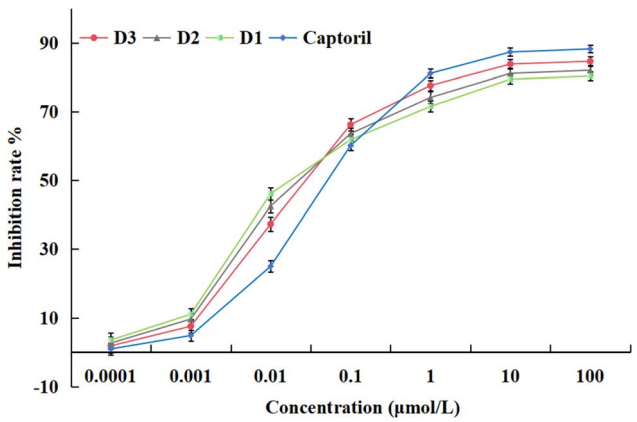

Fig. 13 Inhibitory effect of designed peptides and captoril on ACE activity.

4 Conclusion

The aim of the present study is to use the above mentioned 150 tri-peptides to identify the required structural features affecting the ACE inhibitory activities by a combination of several *in silico* approaches. The 3D-QSAR models were developed on this series of ACE tri-peptides using CoMFA and CoMSIA methods. As far as we know, this study provides the first 3D-QSAR study for this series of ACE inhibitory peptides. Although Aluko *et al.*[29] have studied the quantitative structure–activity relationship of 140 ACE tri-peptides, only models using partial least squares regression were computed, ignoring the three dimensional conformation. In addition, we have found that other studies of ACE tripeptides have applied different data, for example, Zhang *et al.*[48] have employed 3D-QSAR, molecular docking and activity evaluation to study the bioactivities of ACE-inhibitory peptides with phenylalanine C-terminus. A series of ACE-inhibitory (ACEi) peptides with tryptophan C-terminal in aqueous solutions were also studied using 3D-QSAR, molecular docking and molecular dynamics (MD) simulation by Zhang *et al.*.[49] Furthermore, some QSAR researches were mainly focused on food-derived ACE inhibitory peptides.[50] In our work, all the constructed models were found to have excellent internal and external values, indicating that the models are statistically reliable. The overall contour plot analyses reveal that steric, electrostatic, hydrophobic, and hydrogen bond acceptor fields are found to be critical for improving the ACE inhibitory activity.

Molecular docking was also employed to study the binding interactions between peptides and the ACE receptor, and the docking results are consistent with those contours obtained by the 3D-QSAR models. The findings hint that the tri-peptides are

© 2025 The Author(s). Published by the Royal Society of Chemistry

Open Access Article. Published on 21 October 2025. Downloaded on 1/22/2026 4:50:41 AM. This article is licensed under a Creative Commons Attribution-NonCommercial 3.0 Unported Licence.

mainly stabilized by hydrogen bonds interactions with Gln281, Glu376, Glu384, Asp415, Lys511, Tyr520, Tyr523. This is in accord with the results derived from ref. 51, the molecular docking indicates that the compounds form hydrogen bonds with Glu384, Gln281, Tyr520, Lys511, which play an important role in stabilizing the peptide-ACE complex, this is consistent with the conclusions we have reached, further suggesting the accuracy of molecular docking.

Overall, all the findings are very useful for designing novel tri-peptides targeting ACE, three new peptides were predicted using CoMFA and CoMSIA-SHA models. The results of molecular docking indicate that the newly predicted peptides are more stable in the binding pocket of ACE than the most active peptide 144. At the same time, we have synthesized the designed peptides, and the ACE inhibitory activity was tested using *in vitro* experiments. The peptide D3 has the most potent ACE inhibitory activity ($IC_{50} = 0.078$ μmol). Overall, the results of this study provide a new idea for the development of higher ACE inhibitory peptides.

Author contribution

All authors contributed to the study conception and design. Conceptualization and writing – original draft was performed by Fangfang Wang and Shanli Peng. The 3D-QSAR models were developed by Fenglin Jiao and Jinlin Yang . Software and visualization were performed by Bo Zhou. All authors read and approved the final manuscript.

Conflicts of interest

The authors declare that there are no conflicts of interest.

Data availability

The datasets generated during and/or analyzed during the current study are available from the corresponding author on reasonable request.

Supplementary information is available. See DOI: **https://doi.org/10.1039/d5ra06104k**.

Acknowledgements

The study was supported by the National Natural Science Foundation of China (no. 32001699) and the National College Students' innovation and entrepreneurship training program (202510452024).

References

1 M. Zhang, *et al.*, Prevalence, awareness, treatment, and control of hypertension in China, 2004-18: findings from six rounds of a national survey, *Bmj*, 2023, **380**, 1–12.
2 J. Moore, Hypertension: catching the silent killer, *Nurse Pract. Am. J. Prim Health Care*, 2005, **30**(10), 16–35.
3 Jr, J. L. Izzo and M. R. Weir, Angiotensin-converting enzyme inhibitors, *J. Clin. Hypertens.*, 2011, **13**(9), 667.
4 K. Hanif, H. K. Bid and R. Konwar, Reinventing the ACE inhibitors: some old and new implications of ACE inhibition, *Hypertens. Res.*, 2010, **33**(1), 11–21.
5 L. T. Skeggs, J. R. Kahn and N. P. Shumway, The preparation and function of the hypertensin-converting enzyme, *J. Trace Elem. Exp. Med.*, 1956, **103**(3), 295.
6 E. M. Lonn, *et al.*, Emerging role of angiotensin-converting enzyme inhibitors in cardiac and vascular protection, *Circulation*, 1994, **90**(4), 2056–2069.
7 D. P. Bicket, Using ACE inhibitors appropriately, *Am. Fam. Physician*, 2002, **66**(3), 461–469.
8 R. W. Piepho, Overview of the angiotensin-converting-enzyme inhibitors, *Am. J. Health Syst. Pharm.*, 2000, **57**(suppl_1), S3–S7.
9 B. M. Elhaj, F. H. Farah and H. S. Ali, Captopril: An Overview of Discovery, Development, and Post-marketing Surveillance as an Effective Anti-hypertensive Drug, *Acta sci. pharm. sci.*, 2021, **5**(4).
10 K. Simpson and B. Jarvis, Lisinopril: a review of its use in congestive heart failure, *Drugs*, 2000, **59**(5), 1149–1167.
11 H. Shionoiri, *et al.*, Fosinopril: clinical pharmacokinetics and clinical potential, *Clin. Pharmacokinet.*, 1997, **32**(6), 460–480.
12 M. Polakovičová and J. Jampílek, Advances in structural biology of ACE and development of domain selective ACE-inhibitors, *Med. Chem.*, 2019, **15**(6), 574–587.
13 H. Ahmad, *et al.*, Angiotensin-converting enzyme and hypertension: a systemic analysis of various ACE inhibitors, their side effects, and bioactive peptides as a putative therapy for hypertension, *J. Renin-Angiotensin-Aldosterone Syst. JRAAS*, 2023, **2023**, 7890188–7890196.
14 S. H. Mahmoudpour, *et al.*, Pharmacogenetics of ACE inhibitor-induced angioedema and cough: a systematic review and meta-analysis, *Pharmacogenomics*, 2013, **14**(3), 249–260.
15 D. Y. Pujiastuti, *et al.*, Marine organisms as potential sources of bioactive peptides that inhibit the activity of angiotensin I-converting enzyme: a review, *Molecules*, 2019, **24**(14), 2541.
16 H. Dai, *et al.*, Discovery of ACE inhibitory peptides derived from green coffee using in silico and in vitro methods, *Foods*, 2023, **12**(18), 3480.
17 T. Panyayai, *et al.*, The potential peptides against angiotensin-I converting enzyme through a virtual tripeptide-constructing library, *Comput. Biol. Chem.*, 2018, **77**, 207–213.
18 S. H. Ferreira, D. C. Bartelt and L. J. Greene, Isolation of bradykinin-potentiating peptides from Bothrops jararaca venom, *Biochemistry*, 1970, **9**(13), 2583–2593.
19 S. Engel, *et al.*, Effects of the nonapeptide SQ 20881 on blood pressure of rats with experimental renovascular hypertension, *Proc. Soc. Exp. Biol. Med.*, 1973, **143**(2), 483–487.
20 E. Muirhead, B. Brooks and K. Arora, Prevention of malignant hypertension by the synthetic peptide SQ 20,881, *Lab Invest.*, 1974, **30**(2), 129–135.
21 G. Oshima, H. Shimabukuro and K. Nagasawa, Peptide inhibitors of angiotensin I-converting enzyme in digests of

© 2025 The Author(s). Published by the Royal Society of Chemistry

Open Access Article. Published on 21 October 2025. Downloaded on 1/22/2026 4:50:41 AM. This article is licensed under a Creative Commons Attribution-NonCommercial 3.0 Unported Licence.

gelatin by bacterial collagenase, *Biochim. Biophys. Acta Enzymol.*, 1979, **566**(1), 128–137.
22 Y. Nakamura, *et al.*, Antihypertensive effect of sour milk and peptides isolated from it that are inhibitors to angiotensin I-converting enzyme, *J. Dairy Sci.*, 1995, **78**(6), 1253–1257.
23 K. Majumder and J. Wu, A new approach for identification of novel antihypertensive peptides from egg proteins by QSAR and bioinformatics, *Food Res. Int.*, 2010, **43**(5), 1371–1378.
24 H.-L. He, D. Liu and C.-B. Ma, Review on the angiotensin-I-converting enzyme (ACE) inhibitor peptides from marine proteins, *Appl. Biochem. Biotechnol.*, 2013, **169**, 738–749.
25 I. W. Cheung, *et al.*, Angiotensin-I converting enzyme inhibitory activity of hydrolysates from oat (Avena sativa) proteins by in silico and in vitro analyses, *J. Agric. Food Chem.*, 2009, **57**(19), 9234–9242.
26 R. He, *et al.*, Purification and hypotensive activity of rapeseed protein-derived renin and angiotensin converting enzyme inhibitory peptides, *J. Funct.Foods*, 2013, **5**(2), 781–789.
27 G. Oshima and K. Nagasawa, Stereospecificity of peptidyl dipeptide hydrolase (angiotensin I-converting enzyme), *J. Nutr. Biochem.*, 1979, **86**(6), 1719–1724.
28 S. Zhu, *et al.*, Trends in application of advancing computational approaches in GPCR ligand discovery, *Exp. Biol. Med.*, 2021, **246**(9), 1011–1024.
29 J. Wu, R. E. Aluko and S. Nakai, Structural requirements of angiotensin I-converting enzyme inhibitory peptides: Quantitative structure–activity relationship study of di-and tripeptides, *J. Agric. Food Chem.*, 2006, **54**(3), 732–738.
30 U. Bütikofer, *et al.*, Quantification of the angiotensin-converting enzyme-inhibiting tripeptides Val-Pro-Pro and Ile-Pro-Pro in hard, semi-hard and soft cheeses, *Int. Dairy J.*, 2007, **17**(8), 968–975.
31 Y.-K. KIM, *et al.*, Novel angiotensin-I-converting enzyme inhibitory peptides derived from recombinant human αs1-casein expressed in Escherichia coli, *J. Dairy Res.*, 1999, **66**(3), 431–439.
32 D. K. Layman and J. I. Baum, The emerging role of dairy proteins and bioactive peptides in nutrition and health, *J. Nutr.*, 2004, **134**, S968–S973.
33 M. Clark, R. D. Cramer and N. Van Opdenbosch, Validation of the general purpose tripos 5.2 force field, *J. Comput. Chem.*, 1989, **10**(8), 982–1012.
34 W. P. Purcell and J. A. Singer, A brief review and table of semiempirical parameters used in the Hueckel molecular orbital method, *J. Chem. Eng. Data*, 1967, **12**(2), 235–246.
35 R. D. Cramer, D. E. Patterson and J. D. Bunce, Comparative molecular field analysis (CoMFA). 1. Effect of shape on binding of steroids to carrier proteins, *J. Am. Chem. Soc.*, 1988, **110**(18), 5959–5967.
36 G. Klebe, U. Abraham and T. Mietzner, Molecular similarity indices in a comparative analysis (CoMSIA) of drug molecules to correlate and predict their biological activity, *J. Med. Chem.*, 1994, **37**(24), 4130–4146.
37 A. Khaldan, *et al.*, Computational study of quinoline-based thiadiazole compounds as potential antileishmanial inhibitors, *New J. Chem.*, 2022, **46**(36), 17554–17576.
38 S. Wold, *et al.*, The collinearity problem in linear regression. The partial least squares (PLS) approach to generalized inverses, *SIAM J. Sci. Stat. Comput.*, 1984, **5**(3), 735–743.
39 K. Roy, S. Kar and P. Ambure, On a simple approach for determining applicability domain of QSAR models, *Chemom. Intell. Lab. Syst.*, 2015, **145**, 22–29.
40 D. Gadaleta, *et al.*, Applicability domain for QSAR models: where theory meets reality, *Int. J. Quant. Struct.-Prop. Relat.*, 2016, **1**(1), 45–63.
41 S. A. Halim, *et al.*, Targeting dengue virus NS-3 helicase by ligand based pharmacophore modeling and structure based virtual screening, *Front. Chem.*, 2017, **5**, 88.
42 P. Tue-Ngeun, *et al.*, Binding interactions and in silico ADME prediction of isoconessimine derivatives as potent acetylcholinesterase inhibitors, *J. Mol. Graph. Model.*, 2024, **129**, 108746.
43 U. C. Singh and P. A. Kollman, An approach to computing electrostatic charges for molecules, *J. Comput. Chem.*, 1984, **5**(2), 129–145.
44 G. M. Morris, *et al.*, AutoDock4 and AutoDockTools4: Automated docking with selective receptor flexibility, *J. Comput. Chem.*, 2009, **30**(16), 2785–2791.
45 G. L. Warren, *et al.*, A critical assessment of docking programs and scoring functions, *J. Med. Chem.*, 2006, **49**(20), 5912–5931.
46 B. Kramer, M. Rarey and T. Lengauer, Evaluation of the FLEXX incremental construction algorithm for protein–ligand docking, *Proteins: Struct., Funct., Bioinf.*, 1999, **37**(2), 228–241.
47 Z. Li, *et al.*, Preparation and Vasodilation Mechanism of Angiotensin-I-Converting Enzyme Inhibitory Peptide from Ulva prolifera Protein, *Mar. Drugs*, 2024, **22**(9), 398.
48 C. Qi, *et al.*, Studies on the Bioactivities of ACE-inhibitory Peptides with Phenylalanine C-terminus Using 3D-QSAR, Molecular Docking and in vitro Evaluation, *Mol. Inf.*, 2017, **36**(9), 1600157.
49 W. Yan, *et al.*, Studies on molecular mechanism between ACE and inhibitory peptides in different bioactivities by 3D-QSAR and MD simulations, *J. Mol. Liq.*, 2020, **304**, 112702.
50 V. R. Vukic, *et al.*, In silico identification of milk antihypertensive di-and tripeptides involved in angiotensin I–converting enzyme inhibitory activity, *Nutr. Res.*, 2017, **46**, 22–30.
51 J.-B. Tong, *et al.*, QSAR studies of angiotensin converting enzyme inhibitors using CoMFA, CoMSIA and molecular docking, *J. Serb. Chem. Soc.*, 2021, **86**(5), 469–482.

© 2025 The Author(s). Published by the Royal Society of Chemistry